arXiv:1701.02949v1 [cond-mat.str-el] 11 Jan 2017

Additional energy scale in SmB_6 at low temperature

L. Jiao,[1] S. Rößler,[1] D. J. Kim,[2] L. H. Tjeng,[1] Z. Fisk,[2] F. Steglich,[1] and S. Wirth[1]

[1] *Max-Planck-Institute for Chemical Physics of Solids, Nöthnitzer Str. 40, 01187 Dresden, Germany*
[2] *Department of Physics and Astronomy, University of California, Irvine, CA 92697*

(Dated: January 12, 2017)

Topological insulators give rise to exquisite electronic properties due to their spin-momentum locked Dirac-cone-like band structure. Recently, it has been suggested that the required opposite parities between valence and conduction band along with strong spin-orbit coupling can be realized in correlated materials. Particularly, SmB_6 has been proposed as candidate material for a topological Kondo insulator. By utilizing scanning tunneling microscopy and spectroscopy measurements down to 0.35 K, we observed several states within the hybridization gap of about ±20 meV on well characterized (001) surfaces of SmB_6. The spectroscopic response to impurities and magnetic fields allows to distinguish between dominating bulk and surface contributions to these states. The surface contributions develop particularly strongly below about 7 K which can be understood in terms of a breakdown of the Kondo effect at the surface. Our high-resolution data provide detailed insight into the electronic structure of SmB_6, which will reconcile many current discrepancies on this compound.

In the past few years, the concept of strong topological insulators which exhibit an odd number of surface Dirac modes characterized by a $\mathbb{Z}_2$ topological index, has attracted great interest. In this context, it was theoretically predicted that some Kondo insulators, such as SmB_6, $Ce_3Bi_4Pt_3$, CeNiSn, $CeRu_4Sn_6$, are candidates for strong three-dimensional (3D) topological insulators [1, 2]. In particular, SmB_6 is intensively studied due to its simple crystal structure and clear signatures of a hybridization gap. Theoretically, a common picture of the multiplet f-states and the Kondo coupling is shared among different band structure calculations for bulk SmB_6 [2–7], as sketched in Fig. 1. Due to strong spin-orbit coupling and crystal field effects, the f-states of Sm are split into several multiplets as presented in Fig. 1a. Considering the symmetry of the multiplets, only the Γ_7 and $\Gamma_8^{(1)}$ bands are allowed to hybridize with the Sm d-band via the Kondo effect [4, 6]. As a result, two hybridization gaps (Δ_1, Δ_2) may open at different energies as sketched in Fig. 1b (in principle only Δ_2 is a well-defined gap). Although topological surface states (TSS) are unambiguously predicted to reside within the hybridization gap [2–7], no consensus has been reached on the structure of the TSS around the Fermi energy (E_F). Nonetheless, the prediction of TSS provides an attractive explanation for the four decades-old conundrum [8] of SmB_6 which exhibits a plateau in the resistivity typically below about 5 K [9, 10].

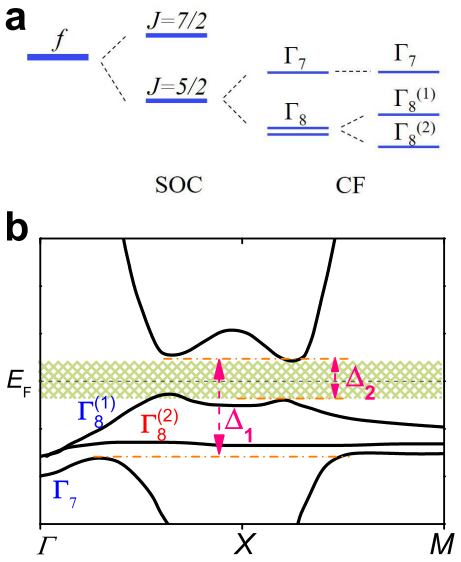

FIG. 1. **Sketch of the multiplet f-states and the resulting band structure.** (**a**) Evolution of energy levels of the f-states in SmB_6, which follows from the work of Ref. [6, 7]. The f-states are split into $J = 7/2$ and $J = 5/2$ states by spin-orbit coupling (SOC). The $J = 5/2$ state, which is slightly below E_F, is split into a Γ_7 doublet and a Γ_8 quartet by the crystal field (CF). Away from the Γ point, the Γ_8 quartet is further split into $\Gamma_8^{(1)}$ and $\Gamma_8^{(2)}$ doublets. (**b**) A schematic bulk band structure of SmB_6 based on calculations of Ref. [2–7]. Hybridization between the Γ_7, $\Gamma_8^{(1)}$ bands and the conduction band opens two gaps which are denoted as Δ_1 (typically around 20 meV) and Δ_2. The shaded area marks the small bulk gap which may host in-gap states. See also Supplementary Fig. 1 for details.

Experimentally, the existence of metallic surface states below about 5 K has been best illustrated by electrical transport measurements on SmB_6 [10–12]. However, the *origin* of these surface states and their topological properties remain controversial in spite of intensive investigations. Several properties of SmB_6 interfere with a straightforward interpretation. One major issue arises with respect to the size of the hybridization gap. Spectroscopic measurements observed a large hybridization gap of about 15–20 meV [13–24], which is normally understood by considering a single coherent f-band

hybridizing with a conduction band (Supplementary Fig. 1). Typically, additional features within this energy scale are assumed to be in-gap states. In some cases, the in-gap states are further ascribed to TSS [15, 17]. On the other hand, analyses of thermal activation energies derive a small excitation energy of 2–5 meV, which shows bulk properties and is understood in terms of a small, likely indirect, bulk gap [25–27] or in-gap states [28–30]. Obviously, different probes as well as different ranges in the measurement temperatures reveal only either the bigger or the smaller hybridization gap sketched in Fig. 1b. Nevertheless, these measurements provide essential constraints to the sizes of the two hybridization gaps. In terms of topology (*i.e.* trivial or non-trivial surface states), experimental results, even obtained by using the very same method, are conflicting among many reports [14–24, 31–34]. Considering the exotic phenomena which appear only within ±20 meV and below 5 K, measurements with very high energy resolution and at very low temperature are highly desired.

Another severe difficulty, which contributes to such a wide discrepancy among the experimental results, is caused by the surface itself. Specifically, the (001) surface of SmB_6 is polar [23]. This can induce different types of band bendings [14], quantum well confinements [35], charge puddles, and surface reconstructions [36–39]. Specifically the latter may give rise to conducting surface layers on its own [23]. Frequently, different types of surfaces (B- and Sm-terminated, reconstructed and non-reconstructed) coexist at different length scales on one and the same cleaved surface which may complicate interpretation of spectroscopic results, *e.g.*, by angle-resolved photoemission spectroscopy (ARPES).

We therefore conducted scanning tunneling microscopy/spectroscopy (STM/STS) down to the base temperature of 0.35 K with an energy resolution of about 0.5 meV. This allowed us to identify the fine structure of the hybridization gaps on large and non-reconstructed surfaces in the sub-meV scale. Moreover, by measuring the impurity, magnetic-field and temperature dependence of the STS spectra, we were able to attribute bulk and/or surface contributions to these states, and unveil a new energy scale of $\simeq 7$ K, which provides an important piece of the puzzle for a unified picture of SmB_6.

RESULTS

Topography and STS spectra at base temperature. In Fig. 2b, the topography of a non-reconstructed surface with clear atomic resolution is presented. The distance of about 4.1 Å and arrangement of the corrugations is in good agreement with the lattice constant $a = 4.133$ Å of the cubic crystal structure of SmB_6 (Fig. 2a). The very small number of defects compared to the number of unit cells within the field of view (more than 5200) not only indicates high sample quality but also ensures that the measured spectrum is not influenced by defects. The absence of any corrugation other than along the main crystallographic axes, as nicely seen in the inset to Fig. 2b, clearly indicates a B-terminated surface [37, 39].

The tunneling conductance $g(V) \equiv \mathrm{d}I(V)/\mathrm{d}V$, measured at $T = 0.35$ K and far away from any impurity, exhibits several anomalies close to E_F, marked by i) – v) in Fig. 2c. A change in the slope of $g(V)$ around ±20 meV suggests a pronounced loss of local density of states (LDOS) within this energy range. Around the same energy, the opening of a gap has been widely observed by a number of spectroscopic tools as mentioned above [16–24], including STS [36–38]. Based on the band structure displayed in Fig. 1b, the kinks marked by i) can be ascribed to the Kondo coupling between the f-band and the conduction band, which results in a decreased conduction electron density inside the hybridization gap below the Kondo temperature T_K [40].

More importantly, we were able to disentangle several anomalies which were hitherto not resolved *individually* by STS at higher temperature [36–38]. Benefitting from this improvement, we can investigate the fine structure of bulk/surface bands and go beyond a simple Kondo hybridization analysis of the bulk states, which is based on only one f-band and one conduction band [14]. Around −13.5 meV, there is a small peak marked by ii). Excitations with similar energy have been reported before, *e.g.* by ARPES (−15 meV) [15], X-ray photoelectron spectroscopy (XPS) (−15 meV) [14] and inelastic neutron scattering (14 meV) [41, 42], yet with differing explanations as to its origin. As discussed below, this small peak is most likely related to the indirect tunneling into the localized $\Gamma_8^{(2)}$ states. Compared to delocalized f-states, such localized f-states may give rise to only small anomalies in spectroscopy measurements [43].

Compared to peak ii), peak iii) (at around −6.5 meV) is very sharp and pronounced. Such a peak has been observed on different types of surfaces, including reconstructed ones [36–38], which clearly indicates that there are significant bulk contributions to this state. Very likely, the weakly dispersive structure of the hybridized $\Gamma_8^{(1)}$ band around the X-point along with the Fano effect can induce a peak in the conductance spectra at this energy level. In a Kondo system, the Fano effect is due to a quantum mechanical interference of electrons tunneling into the localized states and the conduction bands [44, 45]. Either a sharp drop (like feature i)) or a pronounced peak will show up around the gap edge, depending on the tunneling ratio between the two channels as well as the particle-hole asymmetry of the conduction band. However, as has been reported previously, the spectrum deviates from a simple Fano

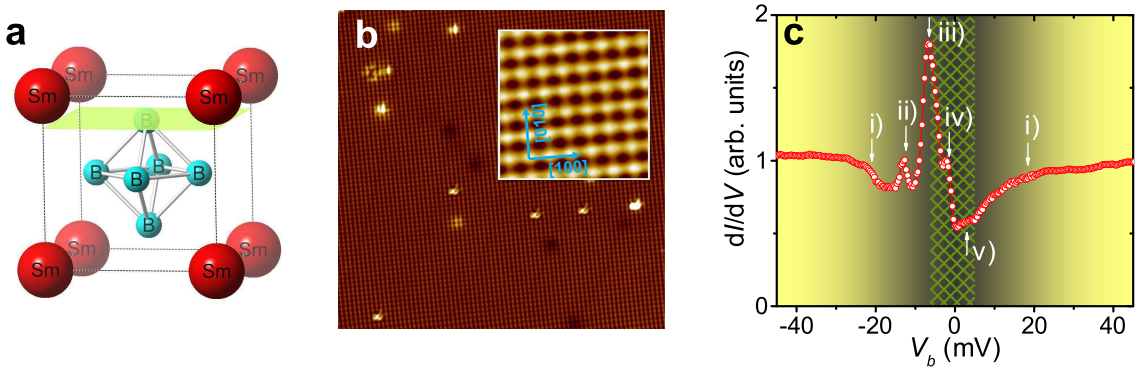

FIG. 2. **B-terminated surface and STS spectra at base temperature.** (**a**) Cubic crystal structure of SmB_6 with lattice constant $a = 4.133$ Å. The green plane indicates a cleave with B-terminated surface. (**b**) STM topography on a 30 × 30 nm^2 non-reconstructed B-terminated surface of SmB_6 ($T = 0.35$ K, bias voltage $V_b = 300$ mV, set-point current $I_{sp} = 400$ pA). Note the small number of defects. For the height scale compare to Fig. 3(**b**). The zoomed inset (3 × 3 nm^2) shows the orientation of the crystallographic axis, clearly indicating B termination. (**c**) Spatially (2×2 nm^2) averaged STS on part of the surface displayed in the inset of (**b**). Several features can clearly be distinguished within ±20 mV, which are marked as i) to v) and discussed in the text. Yellow to gray background in (**c**) indicates the energy range within which the gap opens, while the patterned area marks the region for potential in-gap states. $V_b = 50$ mV, $I_{sp} = 125$ pA, modulation voltage $V_{mod} = 0.2$ mV.

model at low temperature [36, 38], indicating additional components to peak iii) (see also discussion below). This is consistent with our inference that the hybridized $\Gamma_8^{(1)}$ band resides within the big gap Δ_1 and also contributes to the intensity of this peak. Hence, the position of peak iii) can provide an indication with respect to the energy level of the $\Gamma_8^{(1)}$ band and therefore the size of the small gap Δ_2. Note that its energy level is also comparable with the size of the small bulk gap observed by transport measurements [25–27]. Therefore, peak i) to iii) can directly be compared to the band structure in Fig. 1b. To verify the bulk/surface origins of these peaks at low temperature, impurity, magnetic field, and temperature dependence of STS have been conducted. As we will show below, besides bulk components, peak iii) also contains components from the surface layer below 7 K.

Crucially, we also observe small anomalies iv) and v) at ±3 meV, which reside just inside the bulk gap Δ_2 (*cf.* also Fig. 4c and d). The shoulder-like shape of these small anomalies indicates the existence of two weakly dispersive bands or localized states near E_F. It is noted that both features at about ±3 meV also reveal spatial inhomogeneity (see Supplementary Fig. 2), which—given the electronic inhomogeneity of even atomically flat surfaces [39]—hints at a surface origin of these states.

Spatial dependence of the STS spectra. For STM measurements, one possible way to distinguish bulk and surface states is to carefully investigate the tunneling spectra at/near impurities or other defects, because the surface states are more vulnerable to such defects. Therefore, $g(V)$ was measured across two impurity sites at 0.35 K, shown in Figs. 3a and b. The bigger impurity at #A with an apparent height of ≈160 pm is probably located on top of the surface, while the smaller one at #E (apparent height ≈50 pm) is likely incorporated into the crystal. According to Fig. 3c, the $g(V)$-curves are all very similar for positions #B to #F. Even at position #A, *i.e.* on top of the big impurity, the spectrum exhibits similarities; in particular all anomalies i)–v) can be recognized. In addition, a new peak occurs at −10 meV, which may be assigned to an impurity bound state. In Fig. 3d, we plot the height of the peaks ii) to iv) at different positions. A combined analysis of Figs. 3c and d reveals spatial stability of peak ii), being consistent with the expectation for bulk states as discussed above. On the other hand, peaks iii) and iv) are not as stable as peak ii); their heights are suppressed by both the big and the small impurity, which implies that at this temperature both peaks contain contributions from the states pertained to the surface.

Magnetic field dependence of the STS spectra. In Fig. 4a and b, $g(V)$-curves measured at sites #A and #C of Fig. 3a for different applied magnetic fields are presented. There is no distinct change detected up to the maximum field of 12 T for features i) to v), except an enhanced peak amplitude for the impurity state at −10 meV, see Fig. 4b. The magnetic-field independence of these states is consistent with the observation of metallic surface conductance up to 100 T by transport [26, 46–48] and spectroscopic measurements [30, 36]. This observation can be understood by considering a very small g-factor (0.1–0.2) of the f-electrons [49].

Temperature dependence of the STS spectra. We now turn to the temperature dependence of the features i) to v). The temperature evolution of the STS spectra was measured continuously on the same unreconstructed, B-terminated surfaces away from any

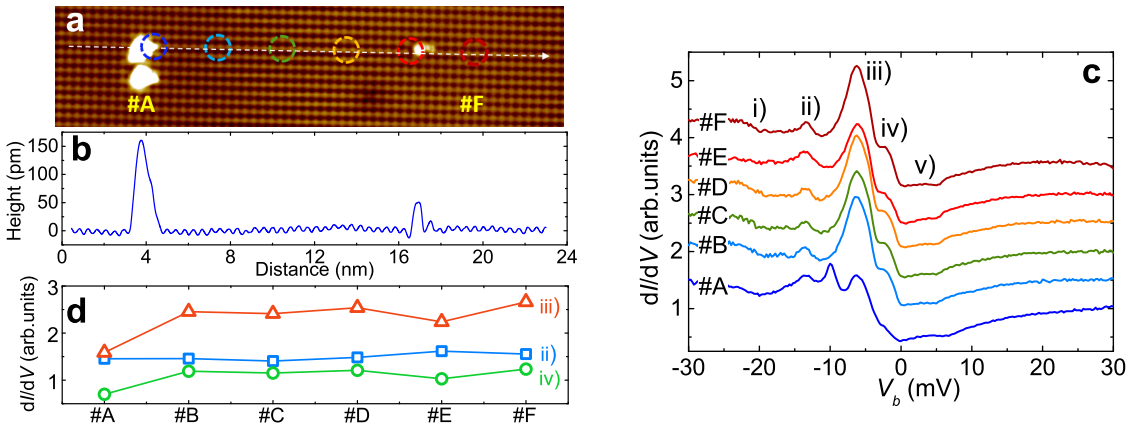

FIG. 3. **Spatial dependence of tunneling spectroscopy.** (**a**) Topography of a non-reconstructed, B-terminated surface (area of 24 × 4 nm^2) with two different types of defects, two large ones at position #A and a smaller one at #E. (**b**) Height scan along the dashed line indicated in (**a**). (**c**) dI/dV-curves measured at six positions (denoted as #A to #F) equally spaced and marked by circles in (**a**). Curves are offset for clarity. T = 0.35 K, V_b = 30 mV, I_{sp} = 100 pA, V_{mod} = 0.3 mV. (**d**) Maximum peak values of the differential conductance at −13.5 mV, −6.5 mV and −3 mV obtained at positions #A to #F.

defect between 0.35 and 20 K, see Fig. 4c. Above 15 K, the spectra show a typical asymmetric lineshape which arises from the Fano effect [44, 45], being in good agreement with previous work [37] (see Supplementary Fig. 4). Upon cooling, the amplitude of peak iii) increases sharply, accompanied by a sudden appearance of peaks iv) and v) below 7 K, with the latter effect being beyond thermal smearing (see Supplementary Fig. 3). The low-temperature evolution of the spectra is clearly seen after the measured $g(V,T)$-curves were subtracted by the data at 20 K, see Fig. 4d. In an effort to quantitatively investigate the evolution of the spectra with temperature, we describe the low-temperature $g(V)$-curves by a superposition of four Gaussian peaks on top of a co-tunneling model (see Supplementary Fig. 4). However, fits to data obtained at higher temperature ($T > 10$ K) turned out to be less reliable (Supplementary Figs. 5 and 6).

To further analyze the temperature evolution of peak iii), we normalized the spectra by its size at $V_b = \pm 30$ mV. The resulting $g(T)$-values of peak iii) are plotted in Fig. 4e. Clearly, a change in the temperature dependence is observed around 7 K. This is further supported by a comparison to data obtained by Yee *et al.* [36] (blue circles and blue dashed line) in a similar fashion but on a (2×1) reconstructed surface (which may explain the scaling factor, right axis). Also, the spectral weights of the −10 meV peak by Ruan *et al.* [38] (green squares) indicate a similar trend at $T \geq 5$ K. Note that even the temperature evolution above about 7 K cannot be explained by a mere thermal broadening effect [36, 38]. By tracing the temperature evolution of the dI/dV-spectra between about 7–50 K [36–38] a characteristic energy scale of about 50 K was derived. This can be accounted for by the Kondo effect of the bulk states, with an additional contribution from a resonance mode [38] which is likely (as discussed above) related to the $\Gamma_8^{(1)}$ state. The same energy scale of $\gtrsim$ 50 K has also been observed by transport [9, 12] and other spectroscopic measurements [13, 20, 50, 51]. However, below 7 K, the intensity of peak iii) shows a sudden enhancement in Fig. 4e, indicating the emergence of an additional energy scale. Considering the fact that this new energy scale as well as many other exotic transport phenomena related to the formation of a metallic surface [10–12] set in simultaneously, the increase in intensity of peak iii) (as well as the appearance of peaks iv) and v)) is expected to rely on the same mechanism that is responsible for the formation of the metallic surface. Both observations appear to evolve out of the bulk phenomena associated with the primary hybridization gap at elevated temperatures. In the following section, we will argue that this new energy scale is related to the breakdown of the Kondo effect at the surface.

DISCUSSION

In this study, the topographic capabilities of the STM allow us to distinguish features i) to v) on non-reconstructed (001) surfaces of a single termination and without apparent defects. Therefore, we can simply exclude the possibility that they are driven by surface reconstructions or defects. Especially the observation of new states on clean surfaces below about 7 K indicates that the exotic properties of SmB_6 are intrinsic rather than due to impurities. The observation of well-resolved

features in our tunneling spectra (discussed above) enables the direct comparison with results of bulk band

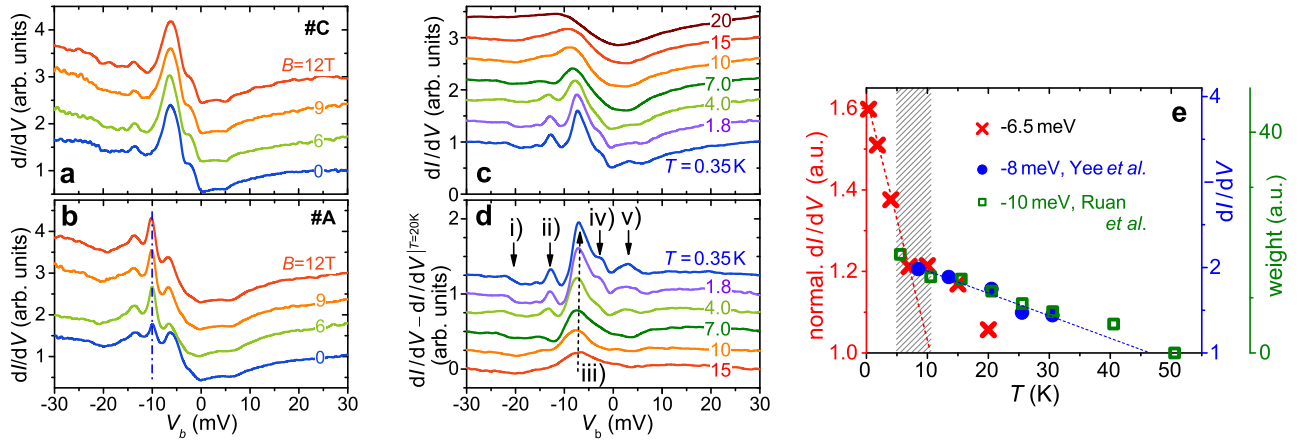

FIG. 4. **Magnetic field and temperature dependence of the STS spectra**. Tunneling spectra measured at magnetic fields up to 12 T and 0.35 K on the top of site (**a**) #C and (**b**) #A (*cf.* Fig. 3**a**). (**c**) Evolution of dI/dV-curves from 0.35 K to 20 K. In order to compare the data, a small linear background is subtract from the raw data. (**d**) Difference tunneling conductance after subtracting the $g(V)$-data measured at 20 K. (**e**) Temperature dependence of the intensity of peak iii). Results for intensities by Yee *et al.* [36] (blue) and spectral weights by Ruan *et al.* [38] (green) are shown for comparison (note matching colors of markers and right axes). Curves are offset for clarity in (**a**)–(**d**). V_b = 30 mV, I_{sp} = 100 pA, V_{mod} = 0.3 mV.

structure calculations [4–7, 18, 52]. This not only reveals the energy levels of the multiplet f-states, but can also reconcile the long-standing debate of 'small' versus 'large' bulk gap in SmB_6 [14]. Consequently, our data shows that a dedicated hybridization model with two—instead of one—multiplet f-states is necessary to interpret the low-energy properties of SmB_6. In particular, peak iii) has multiple components including bulk and surface states, the ratio of which changes dramatically with temperature.

It is widely accepted that the electronic properties of SmB_6 can be divided into several temperature regions, which are based on transport measurements [18, 26] as well as other probes, like ARPES [18, 20]. Apparently, 5-7 K is a crucial regime where the temperature-dependent properties undergo significant changes. Above this range, the electronic states in SmB_6 are governed by the Kondo effect of the bulk [14, 16, 17]. At lower temperatures, several interesting observations—in addition to that of the saturated resistance—were made. For example, the Hall voltage becomes sample-thickness independent [11]; the angular-dependent magnetoresistance pattern changes from fourfold to twofold symmetry [26]; and the development of a heavy fermion surface state is found by magnetothermoelectric measurements [53]. These experimental facts provide convincing evidence for the formation of (heavy) surface states just around 5-7 K, which is in line with the appearance of a new energy scale.

Recently, a surface Kondo breakdown scenario was proposed based on the reduced screening of the local moments at the surface. As a result, the Kondo temperature of the outmost layer (T_K^s) can be strongly suppressed, resulting in a modified band structure [54]. Slab calculations further show that below T_K^s f-electrons gradually become coherent and form weakly dispersive band close to E_F [49, 52]. Remarkably, very narrow peaks with strongly temperature-dependent STS spectra near E_F are regarded as a smoking gun evidence for a surface Kondo breakdown scenario [52]. Based on our experimental results, T_K^s is inferred to be around 7 K, being about an order of magnitude smaller than T_K. The evolution of our tunneling spectra below about 7 K also fit excellently to the theoretical prediction and the related calculations for STS. In such a scenario, the additional component at −6.5 meV and shoulders at ±3 meV are related to the heavy quasiparticle *surface* states, the formation of which supplies an additional tunneling channel in particular into the f-states. This provides a highly possible origin for the metallic surface states and a reasonable explanation to the various experimental observations listed above.

We note that theoretically a surface Kondo breakdown effect does not change the topological invariance of SmB_6, which is determined by the topology of the bulk wave functions. Therefore, the surface-derived heavy quasiparticle states could still be topologically protected. Experimentally, for such topologically protected surface states backscattering is forbidden in quasiparticle interference (QPI) patterns as measured by STM [55]. In line with this prediction and as shown in the Supplementary Fig. 7, no clear QPI pattern could be detected so far from our results, which is similar to the observation by Ruan *et al.*, [38].

METHODS

All samples were grown by the Al-flux method. A cryogenic (base temperature $T \approx 0.35$ K) STM with magnetic field capability of $\mu_0 H \leq 12$ T was utilized. Three SmB_6 single crystals were cleaved a total of five times *in situ* at ≈20 K to expose a (001) surface. Cleaved surfaces were constantly kept in ultra-high vacuum, $p < 3 \cdot 10^{-9}$ Pa. Tunneling was conducted using tungsten tips [56] and the differential conductance ($g(V)$-curve) is acquired by the standard lock-in technique with a small modulation voltage. In our best cleaved sample, the size of non-reconstructed surface can reach to 100×100 nm^2.

In principle, the low-temperature $g(V)$-curves can be well described by a superposition of four Gaussian peaks on top of a Fano model (see example of $g(V, T = 0.35\,\mathrm{K})$ in Supplementary Fig. 4) or more elaborate hybridization models [44, 45] (Supplementary Fig. 6). A similar procedure with only one Gaussian was employed in [38]. However, fits are less reliable at elevated temperature. Instead, our spectra measured at different T in zero field overlap nicely for $V_b < -25$ mV and $V_b > 10$ mV such that they can be normalized by using very similar factors. Consequently, we can directly trace the temperature dependence of the peak height (at least for peak iii)) by measuring the normalized peak intensity as shown in Fig. 4e. Note that the intensities of peak iii) as obtained from Fig. 4d, *i.e.* after subtracting the 20 K-data, yield very similar values as those shown in Fig. 4e from normalized spectra.

ACKNOWLEDGMENTS

We acknowledge valuable discussion with J. W. Allen, P. Coleman, X. Dai, I. Eremin, O. Erten, C.-L. Huang, Deepa Kasinathan, B. I. Min, C. J. Kang, G. Sawatzky, Q. Si and P. Thalmeier. This work was supported by the Deutsche Forschungsgemeinschaft through SPP 1666 and by the Defense Advanced Research Agency (DARPA) under agreement number FA8650-13-1-7374. L.J. acknowledges support by the Alexander-von-Humboldt foundation.

[1] Dzero, M., Sun, K., Galitski, V. & Coleman, P. Topological Kondo Insulators. *Phys. Rev. Lett.* **104**, 106408 (2010).

[2] Alexandrov, V., Dzero, M. & Coleman, P. Cubic Topological Kondo Insulators. *Phys. Rev. Lett.* **111**, 226403 (2013).

[3] Takimoto, T. SmB_6: A Promising Candidate for a Topological Insulator. *J. Phys. Soc. Jpn.* **80**, 123710 (2011).

[4] Lu, F., Zhao, J., Weng, H., Fang, Z. & Dai, X. Correlated Topological Insulators with Mixed Valence. *Phys. Rev. Lett.* **110**, 096401 (2013).

[5] Kim, J.-W. *et al.* Termination-dependent surface in-gap states in a potential mixed-valent topological insulator: SmB_6. *Phys. Rev. B* **90**, 075131 (2014).

[6] Baruselli, P. P. & Vojta, M. Scanning tunneling spectroscopy and surface quasiparticle interference in models for the strongly correlated topological insulators SmB_6 & PuB_6. *Phys. Rev. B* **90**, 201106 (2014).

[7] Kang, C.-L. *et al.* Band Symmetries of Mixed-Valence Topological Insulator: SmB_6. *J. Phys. Soc. Jpn.* **84**, 24722 (2015).

[8] Menth, A., Buehler, E. & Geballe, T. H. Magnetic and Semiconducting Properties of SmB_6. *Phys. Rev. Lett.* **22**, 295-297 (1969).

[9] Allen, J. W., Batlogg, B. & Wachter, P. Large low-temperature Hall effect and resistivity in mixed-valent SmB_6. *Phys. Rev. B* **20**, 4807-4813 (1979).

[10] Kim, D. J., Xia, J. & Fisk, Z. Topological surface state in the Kondo insulator samarium hexaboride. *Nat. Mater.* **13**, 466-470 (2014).

[11] Kim, D. J. *et al.* Surface Hall Effect and Nonlocal Transport in SmB_6: Evidence for Surface Conduction. *Sci. Rep.* **3**, 3150 (2013).

[12] Wolgast, S. *et al.* Low-temperature surface conduction in the Kondo insulator SmB_6. *Phys. Rev. B* **88**, 180405 (2013).

[13] Zhang, X. *et al.* Hybridization, Inter-Ion Correlation, and Surface States in the Kondo Insulator SmB_6. *Phys. Rev. X* **3**, 11011 (2013).

[14] Denlinger, J. D. *et al.* SmB_6 Photoemission: Past and Present. *JPS Conf. Proc.* **3**, 017038 (2014).

[15] Neupane, M. *et al.* Surface electronic structure of the topological Kondo-insulator candidate correlated electron system SmB_6. *Nat. Commun.* **4**, 2991 (2013).

[16] Frantzeskakis, E. *et al.* Kondo Hybridization and the Origin of Metallic States at the (001) Surface of SmB_6. *Phys. Rev. X* **3**, 041024 (2013).

[17] Jiang, J. *et al.* Observation of possible topological in-gap surface states in the Kondo insulator SmB_6 by photoemission. *Nat. Commun.* **4**, 3010 (2013).

[18] Denlinger, J. D. *et al.* Temperature Dependence of Linked Gap and Surface State Evolution in the Mixed Valent Topological Insulator SmB_6. Preprint at http://arxiv.org/abs/1312.6637 (2013).

[19] Xu, N. *et al.* Surface and bulk electronic structure of the strongly correlated system SmB_6 and implications for a topological Kondo insulator. *Phys. Rev. B* **88**, 121102 (2013).

[20] Xu, N. *et al.* Exotic Kondo crossover in a wide temperature region in the topological Kondo insulator SmB_6 revealed by high-resolution ARPES. *Phys. Rev. B* **90**, 085148 (2014).

[21] Xu, N. *et al.* Direct observation of the spin texture in SmB_6 as evidence of the topological Kondo insulator. *Nat. Commun.* **5**, 5566 (2014).

[22] Min, C. *et al.* Importance of Charge Fluctuations for the Topological Phase in SmB_6. *Phys. Rev. Lett.* **112**, 226402 (2014).

[23] Zhu, Z. H. *et al.* Polarity-Driven Surface Metallicity in SmB_6. *Phys. Rev. Lett.* **111**, 216402 (2013).

[24] Hlawenka, P. *et al.* Samarium hexaboride: A trivial surface conductor. Preprint at

http://arxiv.org/abs/1502.01542 (2015).

[25] Cooley, J. C., Aronson, M. C., Fisk, Z. & Canfield, P. C. SmB_6: Kondo Insulator or Exotic Metal? *Phys. Rev. Lett.* **74**, 1629-1632 (1995).

[26] Chen, F. *et al.* Magnetoresistance evidence of a surface state and a field-dependent insulating state in the Kondo insulator SmB_6. *Phys. Rev. B* **91**, 205133 (2015).

[27] Zhou, Y. *et al.* Quantum phase transition and destruction of Kondo effect in pressurized SmB_6. Preprint at http://arxiv.org/abs/1603.05607 (2016).

[28] Gorshunov, B. *et al.* Low-energy electrodynamics of SmB_6. *Phys. Rev. B* **59**, 1808-1814 (1999).

[29] Gabáni, S. *et al.* Properties of the in-gap states in SmB6. *Solid State Commun.* **117**, 641-644 (2001).

[30] Flachbart, K. *et al.* Energy gap of intermediate-valent SmB_6 studied by point-contact spectroscopy. *Phys. Rev. B* **64**, 085104 (2001).

[31] Li, G. *et al.* Two-dimensional Fermi surfaces in Kondo insulator SmB_6. *Science* **346**, 1208-1212 (2014).

[32] Tan, B. S. *et al.* Unconventional Fermi surface in an insulating state. *Science* **349**, 287-290 (2015).

[33] Thomas, S. *et al.* Weak Antilocalization and Linear Magnetoresistance in the Surface State of SmB_6. Preprint at http://arxiv.org/abs/1307.4133 (2013).

[34] Nakajima, Y., Syers, P., Wang, X., Wang, R. & Paglione, J. One-dimensional edge state transport in a topological Kondo insulator. *Nat. Phys.* **12**, 213–217 (2016).

[35] Kang, C.-J. *et al.* Electronic structure of YbB_6: Is it a Topological Insulator or not? *Phys. Rev. Lett.* **116** 116401 (2016).

[36] Yee, M. M. *et al.* Imaging the Kondo Insulating Gap on SmB_6. Preprint at http://arxiv.org/abs/1308.1085 (2013).

[37] Rößler, S. *et al.* Hybridization gap and Fano resonance in SmB_6. *Proc. Natl. Acad. Sci. USA* **111**, 4798-4802 (2014).

[38] Ruan, W. *et al.* Emergence of a Coherent In-Gap State in the SmB_6 Kondo Insulator Revealed by Scanning Tunneling Spectroscopy. *Phys. Rev. Lett.* **112**, 136401 (2014).

[39] Rößler, S., Jiao, L., Kim, D.J., Seiro, S., Rasim, K., Steglich F., Tjeng, L. H., Fisk, Z. & Wirth, S. Surface and electronic structure of SmB_6 through Scanning Tunneling Microscopy. *Phil. Mag.* accepted (2016). doi:10.1080/14786435.2016.1171414.

[40] Ernst, S. *et al.* Emerging local Kondo screening and spatial coherence in the heavy-fermion metal $YbRh_2Si_2$. *Nature* **474**, 362-366 (2011).

[41] Fuhrman, W. T. *et al.* Interaction Driven Subgap Spin Exciton in the Kondo Insulator SmB_6. *Phys. Rev. Lett.* **114**, 036401 (2015).

[42] Alekseev, P. A. *et al.* Magnetic excitation spectrum of mixed-valence SmB_6 studied by neutron scattering on a single crystal. *J. Phys.: Condens. Matter* **7**, 289-305 (1995).

[43] Ramankutty, S.V. *et al.* Comparative study of rare earth hexaborides using high resolution angle-resolved photoemission. *J. Electron. Spectrosc. Relat. Phenom.* **208**, 43-50 (2016).

[44] Maltseva, M., Dzero, M. & Coleman, P. Electron Cotunneling into a Kondo Lattice. *Phys. Rev. Lett.* **103**, 206402 (2009).

[45] Figgins, J. & Morr, D. K. Differential Conductance and Quantum Interference in Kondo Systems. *Phys. Rev. Lett.* **104**, 187202 (2010).

[46] Biswas, S. *et al.* Robust local and non-local transport in the topological Kondo insulator SmB_6 in the presence of high magnetic field. *Phys. Rev. B* **92**, 085103 (2015).

[47] Cooley, J. C. *et al.* High magnetic fields and the correlation gap in SmB_6. *Phys. Rev. B* **52**, 7322-7327 (1995).

[48] Cooley, J. C. *et al.* High Field Gap Closure in the Kondo Insulator SmB_6. *J. Supercond.* **12**, 171-173 (1999).

[49] Erten, O., Ghaemi, P. & Coleman, P. Kondo Breakdown and Quantum Oscillations in SmB_6. *Phys. Rev. Lett.* **116**, 046403 (2016).

[50] Caldwell, T. *et al.* High-field suppression of in-gap states in the Kondo insulator SmB_6. *Phys. Rev. B* **75**, 75106 (2007).

[51] Min, C. H. *et al.* Universal properties of the near-gap spectra of SmB_6: dynamical mean-field calculations and photoemission experiments. Preprint at http://arxiv.org/abs/1511.06325 (2015).

[52] Peters, R., Yoshida, T., Sakakibara, H. & Kawakami, N. Coexistence of light and heavy surface states in a topological multiband Kondo insulator SmB_6. *Phys. Rev. B* **93**, 235159 (2016)).

[53] Luo, Y., Chen, H., Dai, J., Xu, Z. & Thompson, J. D. Heavy surface state in a possible topological Kondo insulator: Magnetothermoelectric transport on the (011) plane of SmB_6. *Phys. Rev. B* **91**, 075130 (2015).

[54] Alexandrov, V., Coleman, P. & Erten, O. Kondo Breakdown in Topological Kondo Insulators. *Phys. Rev. Lett.* **114**, 177202 (2015).

[55] Xu, N., Ding, H. & Shi, M. Spin- and angle-resolved photoemission on the topological Kondo insulator candidate: SmB_6. *J. Phys.: Condens. Matter* **28**, 363001 (2016).

[56] Ernst, S., Wirth, S., Rams, M., Dolocan, V. & Steglich, F. Tip preparation for usage in an ultra-low temperature UHV scanning tunneling microscope. *Sci. Technol. Adv. Mat.* **8**, 347-351 (2007).